Remote Sensing of Environment 173 (2016) 174–186

Contents lists available at ScienceDirect

Remote Sensing of Environment

journal homepage: www.elsevier.com/locate/rse

Examining spectral reflectance features related to foliar nitrogen in forests: Implications for broad-scale nitrogen mapping

Lucie C. Lepine *, Scott V. Ollinger, Andrew P. Ouimette, Mary E. Martin

Earth Systems Research Center, University of New Hampshire, Durham, NH, USA

ARTICLE INFO

Article history:
Received 17 February 2015
Received in revised form 10 November 2015
Accepted 23 November 2015
Available online 5 December 2015

Keywords:
Foliar nitrogen
Canopy nitrogen
Spectral reflectance
Near infrared
AVIRIS
Landsat
MODIS
Spatial resolution
Spectral resolution
Sensor fidelity

ABSTRACT

The concentration of nitrogen (N) in foliage often limits photosynthesis and can influence a number of important biogeochemical processes. For this reason, methods for estimating foliar %N over a range of scales are needed to enhance understanding of terrestrial carbon and nitrogen cycles. High spectral resolution aircraft remote sensing has become an increasingly common tool for landscape-scale estimates of canopy %N because reflectance in some portions of the spectrum has been shown to correlate strongly with field-measured %N. These patterns have been observed repeatedly over a wide range of biomes, opening new possibilities for planned Earth observation satellites. Nevertheless, the effects of spectral resolution and other sensor characteristics on %N estimates have not been fully examined, and may have implications for future analyses at landscape, regional and global scales. In this study, we explored the effects of spectral resolution, spatial resolution and sensor fidelity on relationships between forest canopy %N and reflectance measurements from airborne and satellite platforms. We conducted an exercise whereby PLS, simple and multiple regression calibrations to field-measured canopy %N for a series of forested sites were iteratively performed using (1) high resolution data from AVIRIS (Airborne Visible/Infrared Imaging Spectrometer) that were degraded spectrally from 10 nm to 30 nm, 50 nm, 70 nm, and 90 nm bandwidths, and spatially from 18 m to 30 m and 60 m pixels; (2) data representing Landsat and MODIS (Moderate Resolution Imaging Spectroradiometer) spectral bands simulated with data from AVIRIS; and (3) actual data from Landsat and MODIS. We observed virtually no reduction in the strength of relationships between %N and reflectance when using coarser bandwidths from AVIRIS, but instead saw declines with increasing spatial resolution and loss of sensor fidelity. This suggests that past efforts to examine foliar %N using broad-band sensors may have been limited as much by the latter two properties as by their coarser spectral bandwidths. We also found that regression models were driven primarily by reflectance over broad portions of the near infrared (NIR) region, with little contribution from the visible or mid infrared regions. These results suggest that much of the variability in canopy %N is related to broad reflectance properties in the NIR region, indicating promise for broad scale canopy N estimation from a variety of sensors.

1. Introduction

The concentration of nitrogen (N) in foliage is linked to numerous biogeochemical, physiological and ecological processes and serves as a useful indicator of ecosystem metabolism. Foliar N has been repeatedly identified as a useful predictor of photosynthetic capacity, or A_{max} (Evans, 1989; Field & Mooney, 1986; Reich et al., 1999; Wright et al., 2004); it has been related to stand-level processes such as net primary production (NPP) and canopy light use efficiency (Green, Erickson, & Kruger, 2003; Kergoat, Lafont, Arneth, Le Dantec, & Saugier, 2008; Smith et al., 2002); it provides a widely used measure of herbivore forage quality and susceptibility to defoliation (Jefferies, Klein, & Shaver, 1994; Mattson, 1980; Peeters, 2002); and can provide direct input to ecosystem models (Ollinger & Smith, 2005; Wythers, Reich, Tjoelker, & Bolstad, 2005).

In addition to its influence on carbon assimilation, foliar %N is also tied to the availability of N in soils through mechanisms involving litter decay, net mineralization and plant N uptake (Merilä & Derome, 2008; Ollinger et al., 2002; Parton et al., 2007). This is important given the degree to which humans have perturbed the N cycle globally (e.g., Galloway et al., 2003), and the tendency for N to limit productivity in terrestrial ecosystems (Jandl et al., 2007; Vitousek & Howarth, 1991).

Despite its many important roles, foliar %N is rarely used as a driver in regional- to global-scale analyses. This is, in part, because we lack a reliable means of extending foliar N field measurements to broad-scale spatial patterns. At finer scales (~100–1000 km^2), the capacity for foliar N estimation has been repeatedly demonstrated using high spectral resolution remote sensing instruments, or imaging spectrometers (e.g., Asner & Vitousek, 2005; Coops, Smith, Martin, & Ollinger, 2003; Martin & Aber, 1997; McNeil et al., 2008; Ollinger & Smith,

* Corresponding author.
E-mail address: lucie.lepine@unh.edu (L.C. Lepine).

http://dx.doi.org/10.1016/j.rse.2015.11.028
0034-4257/

2005; Smith, Martin, Plourde, & Ollinger, 2003; Townsend, Foster, Chastain, & Currie, 2003; Wessman, Aber, Peterson, & Melillo, 1988), whose narrow bands can record spectral features that result from electron transitions in pigments and/or are associated with other biochemical constituents in foliage (e.g., Curran, 1989; Curran, Kupiec, and Smith, 1997; Kokaly & Clark, 1999). Martin, Plourde, Ollinger, Smith, and McNeil (2008) further demonstrated that relationships between field-measured %N and canopy spectral properties were strongly driven by NIR reflectance patterns, and were consistent enough across boreal, temperate and tropical forests, to allow development of a single, generalized partial least squares (PLS) equation. Still, application of these methods has been limited because presently available imaging spectrometers have swath widths in the range of 10 km or less and because the potential for similar approaches using other instruments has not been thoroughly tested.

There are at least two potential solutions to this problem. The first is development of a space-based imaging spectrometer capable of providing regional to global coverage. Although planning for such instruments is underway (e.g., HyspIRI; Chien, Silverman, Davies, & Mandl, 2009; National Research Council, 2007), it will likely be years before data become routinely available. A second possibility is to evaluate the degree to which foliar %N might also be estimated using spectral features available from existing sensors that provide broader spatial coverage. Potential for this approach was suggested by Ollinger et al. (2008) and Ollinger (2011) who observed that reflectance over broad portions of the NIR region was strongly correlated with measured %N in temperate and boreal forests, and by Martin et al. (2008) whose generalized partial least squares %N model was most heavily influenced by reflectance across the NIR plateau from 750 nm to 1250 nm. Although there have been other indications that broad-band spectral features contain information related to variability in canopy N (Gamon et al., 1995; Hollinger et al., 2010; Zhao et al., 2005), no studies to date have focused explicitly on how variability in spectral resolution, spatial resolution and sensor fidelity affect foliar N estimation capabilities.

In this study, we examined the influence of spectral resolution, spatial resolution and sensor fidelity on relationships between observed patterns of foliar %N and canopy reflectance. Sensor fidelity refers to the combination of signal-to-noise ratio (SNR), detector uniformity and stability of electronics in an imaging system that together affect the quality of spectra (e.g., Asner et al., 2007; Chen, Ji, Zhou, Chen, & Shen, 2012; Kokaly, Asner, Ollinger, Martin, & Wessman, 2009, Mouroulis & McKerns, 2000). Our analysis draws on a combination of remote sensing and coordinated field measurements from 155 plots within 13 forested research sites across North America. Field measurements were used to evaluate imaging spectrometer data from AVIRIS (high spectral resolution, high spatial resolution, high sensor fidelity); broad-scale sensor data from MODIS (moderate spectral resolution, coarse spatial resolution, high sensor fidelity) and broad-band data from Landsat 5 (coarse spectral resolution, moderate spatial resolution, moderate data fidelity). We also examined relationships between field-measured foliar %N and reflectance in visible and infrared wavelengths on their own, and in several commonly used vegetation indices, in order to evaluate their potential roles in future studies of %N estimation.

2. Methods

2.1. Study sites and field data collection

Our analysis used an existing collection of data from several previous investigations (Ollinger, 2011; Ollinger et al., 2008; Martin et al., 2008) that included thirteen North American research sites representing temperate and boreal evergreen needleleaf and deciduous broadleaf and mixed forests, spanning a range of ages. Site descriptions and sampling dates are given in Table 1.

At each site, samples of sunlit canopy foliage were collected from eight to twenty ~20 × 20 m plots, generally located within a 7 × 7 km area, in conjunction with acquisition of AVIRIS imagery (see Section 2.2.1). Plots were chosen to capture the range of floristic and landscape conditions that occurred over the local landscape at each site. At each plot within each site, sunlit leaves from three or more trees of each dominant and co-dominant species were collected from several heights in the canopy. Leaves were collected either by employing professional tree climbers, by shotgun sampling of small branches (e.g., Smith et al., 2002), or by using telescoping pole pruners where this was sufficient for reaching upper canopy foliage. All foliage samples were oven dried at 70 °C and ground with a Wiley Mill to pass through a 1 mm mesh screen. Analysis for foliar N concentrations, recorded as percent by foliar mass, was conducted with a FOSS NIR spectrometer using methods developed by Bolster, Martin, and Aber (1996).

Converting species-level N concentrations to plot-level mean %N, or whole canopy %N, required estimates of canopy composition, so that foliar N concentrations could be weighted by the fraction of the canopy occupied by each species. Canopy composition at each plot was determined using a camera point-quadrat sampling technique, combined with leaf mass per unit area (LMA) measurements obtained for most of the sites and species we sampled. Where LMA data were not obtained directly (typically for species representing only a small fraction of the canopy), estimates were taken from other published sources (Reich, Kloeppel, Ellsworth, & Walters, 1995; Reich et al., 1999; Smith & Martin, 2001). The camera point-quadrat method employs a 35-mm camera with a telephoto lens used as a range finder (calibrated to distance in meters) and a gridded focusing screen. Using this method, 15 grid point observations at nine sampling stations (plot center and each of the four cardinal and off-cardinal directions at 15 m from plot center) were taken, for a total of 135 observations per plot. LMA data were used to convert fractional leaf area for each species to fractional canopy mass. The camera point-quadrat method has long been used for determining canopy composition and height distributions (Aber, 1979a,b) and has also been shown to produce foliar %N estimates consistent with those calculated with species compositions determined from leaf litterfall collection (Smith & Martin, 2001).

A total of 171 plots were sampled across all sites, with more than 2500 individual foliage samples collected for foliar N analysis. After screening for cloud cover and data quality, a total of 155 field plots were available for comparison with image data. Of these, 43 plots were pure deciduous broadleaf (DBF), 59 were evergreen needleleaf (ENF), and 53 were mixed forest (MF).

2.2. Image data acquisition and processing

2.2.1. AVIRIS

Image data from the Airborne Visible/InfraRed Imaging Spectrometer (AVIRIS) were obtained for all sites between 2001 and 2008 (Table 1). AVIRIS captures upwelling spectral radiance in 224 contiguous wavelengths from 360 to 2500 nm, with a 10 nm nominal bandwidth. For data collections used in this study, AVIRIS was flown on an ER-2 aircraft at approximately 20 km above sea level, producing imagery with a swath width of approximately 11 km, and a pixel size of approximately 18 m. (Details for the sensors used in this analysis are listed in Table 2.)

Field data collection took place within 2–3 weeks of image acquisition whenever possible, although longer lags occurred where constraints were imposed by weather conditions or sensor availability. In a few cases, overflights during the year of field sampling were unsuccessful, but imagery was later obtained from a similar portion of the growing season during a subsequent year. Although less than ideal, we included these data in the analyses because spatial patterns of foliar N were likely to be retained, and also because inter-annual variation in foliar N is typically small relative to the large degree of spatial variation over which we sampled. Nevertheless, some inter-annual variation in

Table 1
Description of sites and dates of image data collection.

Site	Lat. °North	Long. °West	Description	Canopy N (% by mass)[a] mean (range)	Date of imagery (YYYYDOY)		
					AVIRIS	Landsat	MODIS[b]
Austin Cary Memorial Forest, FL	29.74°	82.22°	80-yr slash pine/longleaf pine	1.04 (0.71–1.85)	2002153	2001236	2002185
Donaldson Tract, FL	29.75°	82.16°	25-yr slash pine	1.07 (0.85–1.75)	2002153	2001236	2002185
Bartlett Experimental Forest, NH	44.06°	71.29°	100-yr mixed northern hardwood	1.57 (1.00–2.43)	2003236	2005219	2003217
BERMS, Saskatchewan							
Old Aspen	53.63°	106.20°	85-yr boreal aspen	1.75 (1.56–1.88)	2008203	2008236	2008201
Old Black Spruce	53.99°	105.12°	111-yr boreal black spruce	0.73 (0.66–0.80)	2008203	2008220	
Old Jack Pine	53.92°	104.69°	93-yr boreal Jack pine	0.92 (0.74–1.23)	2008203		
HJP75	53.88°	104.65°	33-yr boreal Jack pine	0.89 (0.77–1.13)	2008203	2007178	2008201
HJP94	53.91°	104.66°	14-yr boreal Jack pine	1.03 (0.80–1.29)	2008203		
HJP02	53.95°	104.65°	6-yr boreal Jack pine	1.14 (0.96–1.42)	2008203		
Catskills Mountains, NY							
Batavia Brook	42.28°	74.11°					
Grog Kill	42.08°	74.27°					
Traver Hollow	42.02°	74.31°					
Biscuit Brook	42.05°	74.49°					
Buttermilk Brook	42.94°	74.41°					
Kanape	42.92°	74.31°					
Campbell River, BC							
Mature Douglas fir	49.87°	125.33°	59-yr temperate evergreen				
Juvenile Douglas fir	49.53°	124.90°	20-yr temperate evergreen				
Regenerating Douglas fir	49.87°	125.29°	8-yr temperate evergreen				
Duke Forest hardwoods, FL	35.97°	79.10°	80–100-yr oak-hickory	1.85 (1.42–2.27)	2002142	2002232	2002137
Duke Forest loblolly pine, FL	35.98°	79.09°	25-yr pine plantation	1.20 (1.15–1.32)	2002142	2002232	2002137
Harvard Forest, MA	42.54°	72.17°	80-yr mixed deciduous	1.78 (1.29–2.20)	2003236	2003175	2003217
Howland Forest, ME	45.20°	68.74°	110-yr boreal evergreen	1.25 (0.84–2.36)	2003236	2003200	2003217
Quebec Boreal Forest							
Mature black spruce	49.69°	74.34°	100-yr boreal black spruce				
Juvenile black spruce	49.76°	74.57°	33-yr boreal black spruce				
Regenerating black spruce	49.27°	74.04°	8-yr boreal black spruce				
Willow Creek, WI	45.81°	90.08°	55–90-yr temperate deciduous	1.74 (1.46–2.09)	2005258	2005239	2005257
Wind River Crane Site, WA	45.82°	121.95°	500-yr temperate evergreen	1.03 (0.88–1.28)	2005263	2005210	2005257

[a] As measured from foliage sampling; see Section 2.1.
[b] 16-day composite MOD43B NBAR product; lat/long coordinates represent center of MODIS 7 × 7 km subset (see Section 2.2.3).

foliar N can occur, so offsets between field and image data collection could represent a potential source of error in the analysis.

All AVIRIS datasets were atmospherically corrected using ImSpec LLC's Atmospheric CORrection Now (ACORN) (v.6). ACORN uses MODTRAN4 radiative transfer code with processing modes specific to calibrated hyperspectral and multispectral data to convert radiance to apparent surface reflectance. AVIRIS data collected prior to 2006 were georegistered to known coordinates collected from GPS measurements, USGS digital orthophotography and NAIP imagery to within 8 m horizontal accuracy. AVIRIS data collected from 2006 to present are orthorectified upon delivery, employing a full three-dimensional ray tracing and digital elevation model. To ensure accurate calibration with our field plots, these

Table 2
Characteristics of sensors used in this study.

Sensor	Data quantization	Spectral range (nm)	No. bands	SNR	Pixel size (m)	Swath width (km)	Reference
AVIRIS[a]	16 bit	365–800	47	1000:1	16–18	11	Green (2005), Platt and Goetz (2004), http://aviris.jpl.nasa.gov/
		800–1300	54	800:1			
		1300–2500	123	300:1			
		Total bands	224				
Landsat 5	8 bit	450–520	1	62:1	30	185	Helder, Ruggles, Dewald, and Madhavan (2004), http://landsat.usgs.gov/about_landsat5.php
		520–600	1	59:1			
		630–690	1	55:1			
		760–900	1	53:1			
		1550–1750	1	29:1			
		2080–2350	1	52:1			
		Total bands	6				
MODIS	12-bit[b]	620–670	1	128:1	250	2330	Xiong, Angal, and Xie (2008), http://modis.gsfc.nasa.gov/about/specifications.php
		841–876	1	201:1			
		459–479	1	243:1	500		
		545–565	1	228:1			
		1230–1250	1	74:1			
		1628–1652	1	275:1			
		2105–2155	1	110:1			
		Total bands	7				

[a] Swath width and pixel size assuming ER-2 aircraft platform.
[b] MODIS data products are scaled to 16-bit.

image data were checked in-house against ground control points and adjusted with a first order polynomial warp when necessary.

NASA's Jet Propulsion Lab routinely performs spectral, radiometric and spatial calibrations on AVIRIS in order to ensure the highest quality data required for science and research applications. As part of the calibration process, AVIRIS signals are analyzed to determine the spectral positions, response functions, and uncertainties of the 224 spectral channels (Green et al., 1998). Adjustments and improvements are incorporated as necessary, which can cause small shifts in band center, full-width at half-maximum (FWHM) and spectral range. For this reason, band centers were not identical in all our datasets, which span a period of eight years. So that all AVIRIS spectral reflectance data could be analyzed together, we resampled all AVIRIS spectra to the spectral band center and FWHM of the most current sensor calibration—here, 2008.

2.2.2. Landsat

Landsat 5 data were obtained for all sites from the USGS through the National Land Archive Production System (NLAPS). Landsat 5 imagery was chosen over Landsat 7 because of the scan line corrector (SLC) failure on Landsat 7 (e.g., Pringle, Schmidt, & Muir, 2009). Landsat 5 operates in a sun synchronous, near polar orbit with a swath width of 185 km and a repeat cycle of 16 days. Landsat 5 has six reflective bands with spatial resolution of 30 m, and one thermal band with 120 m spatial resolution. We sought to obtain Landsat 5 scenes that corresponded as closely to field sampling dates as possible, although scenes that were cloud-free over the research sites for these dates were available for only half the sites. For the remainder, we chose cloud-free scenes during the peak growing season from within a year of field data collection (see Table 1). All Landsat 5 scenes were downloaded in GEOTIFF format as terrain-corrected (L1T) calibrated radiance images (U.S. Geological Survey, 2011). As with the AVIRIS imagery, we used the ACORN software to transform radiance to apparent surface reflectance, and verified positional accuracy with known field, vector and image coordinates. Only the six reflective bands were used in our analysis; the thermal band was excluded (see Table 2).

2.2.3. MODIS

The MODerate-resolution Imaging Spectroradiometer (MODIS) instruments operate on two sun synchronous orbiting spacecraft—Terra and Aqua. MODIS has a viewing swath width of ~2330 km and detectors that measure 36 spectral bands between 0.405 and 14.385 μm at varying bandwidths and spatial resolutions (see Table 2). Bands 1–7 are used primarily for studies of land, cloud and aerosol properties. Reflectance from these seven bands are used to generate the MODIS nadir BRDF-adjusted reflectance (NBAR) data product, a 16-day composite that combines data from both Terra and Aqua and uses a bidirectional reflectance distribution function (BRDF) to model the values from anywhere on the globe as if they were taken from nadir view (Schaaf et al., 2002).

MODIS NBAR is among the MODIS Land Product Subsets freely available from the Oak Ridge National Laboratory Distributed Active Archive Center (ORNL DAAC, 2011) for a network of flux towers and research sites around the world. The subsets cover a 7 × 7 km area, and were readily available for all sites in this study. We chose the 16-day composite data product that best matched the time period captured by AVIRIS and our field-data collections. All together, a total of 27 MODIS subsets were obtained for our study sites (Table 1). Because the MODIS NBAR product is a georeferenced reflectance data product, it required no post-processing upon delivery.

2.3. Estimation of canopy nitrogen concentration

2.3.1. AVIRIS

Reflectance spectra were extracted from AVIRIS imagery for all field plot locations, resulting in a spectral calibration dataset of 155 field-measured canopy %N values and matching reflectance spectra. Following methods described in Martin et al. (2008), measured %N for each plot was related to AVIRIS reflectance spectra through partial least squares (PLS) regression (discussed below) to derive a predictive model. The leave-one-out method of cross-validation was used to develop the model (calibration) as well as to derive predicted vs. observed (validation) statistics.

We used the Martin et al. (2008) PLS calibration method applied to the entire AVIRIS data set to set a benchmark for canopy N detection accuracy. To determine how a loss in spectral resolution affects canopy %N estimates, we then degraded AVIRIS image spectral resolution to progressively wider spectral bands—from 10 nm (the nominal spectral bandwidth of AVIRIS data) to 30 nm, 50 nm, 70 nm, and 90 nm bandwidths—and repeated the PLS calibration. As with the initial PLS regression described above, each of the four iterations using degraded spectral resolution incorporated data from all sites into one generalized model for comparison against the 10 nm benchmark model.

Best-fit PLS regression models were those that minimized the number of factors and calibration/validation errors, as determined by leave-one-out cross validation statistics. Accuracy and precision of PLS regression models were compared with the coefficient of determination (r^2), root mean squared error (RMSE) and prediction error sum of squares (PRESS RMSE) statistics. The RMSE provided a measure of the standard deviation of the error in the whole model predictions; the PRESS RMSE tested how well the model predicted each of the points in the data set if they were not included in the regression (a small PRESS RMSE indicates that the model is not overly sensitive to any single data point).

To test the influence of specific spectral regions on estimates of canopy %N, we also performed a series of standard least square regressions of reflectance on %N. We tested narrow (10 nm) and spectrally coarsened wavelengths within the visible (~450–750 nm), near infrared (~800−1250 nm) and mid-infrared (~1300–2500 nm) regions of the spectrum, as well as simulated spectral bands from Landsat and MODIS sensors, in a series of regressions of reflectance against canopy %N. Specifically, we used stepwise regression and simple linear regression as a means of examining the influence of various spectral regions. Spectral reflectance from AVIRIS wavelengths and AVIRIS-simulated Landsat and MODIS wavelengths were entered, respectively, into forward stepwise models with a probability threshold of 0.05 to enter—i.e., the maximum p-value that an effect (wavelength) must have to be entered into the model during a forward step. The stopping rule for the stepwise model was a minimum Bayesian information criterion (BIC) and low prediction error sum of squares (PRESS) statistics. Individual wavelengths were also iteratively entered into simple linear regressions against %N. The predictive strength of the stepwise multiple regressions and simple regressions was assessed with r^2, RMSE and PRESS statistics, as described above. Regression results with low reported RMSE and PRESS RMSE values indicated best fit models in our analyses.

Using nominal and spectrally degraded AVIRIS reflectance data, and AVIRIS-simulated Landsat and MODIS data, we also calculated four commonly used vegetation indices—DVI (the difference vegetation index; [NIR − red]); RVI (the ratio vegetation index; [NIR/red]); NDVI (the normalized difference vegetation index; [NIR − red]/[NIR + red]); and EVI (the enhanced vegetation index; [2.5 ∗ NIR − red]/[1 + NIR + 6red − 7.5blue])—and compared their relationships to canopy %N using simple linear regression analyses. Simulating Landsat and MODIS sensor data with AVIRIS allowed us to examine the utility of wavelengths detected by these sensors, but at high spatial resolution and high sensor fidelity.

In addition to assessing the utility of vegetation indices for estimating canopy %N (e.g., Ferwerda, Skidmore, & Mutanga, 2005; Kruse, Christians, & Chaplin, 2006) the indices also served as a means for representing variability in leaf area index (LAI) and biomass relative to %N. As discussed in Section 2.1, field data used in this study were collected as part of several previous field campaigns, and did not include any

new field measurements. Because plot-level LAI measurements were available for less than a quarter of all the plots in this analysis (and varied by method of LAI measurement), the vegetation indices we chose represent reasonable proxies for LAI and biomass to compare to canopy %N.

In order to assess the effect of spatial resolution on spectral estimation of canopy %N, AVIRIS data were spatially degraded to 30 m (e.g., Landsat pixel size) and 60 m (e.g., planned HyspIRI pixel size) only—i.e., no coarser than 60 m. We felt comfortable with some deviation between plot size (20 × 20 m field plots) and pixel resolution because an important criterion for plot selection was that plots be located within larger blocks of the same forest type, away from edges and shifts in composition. Effects of spatial resolution were explored further with Landsat and MODIS data (described below).

2.3.2. Landsat

As with AVIRIS imagery, we extracted reflectance spectra associated with each of the field plots from each corresponding Landsat scene. Reflectance from the six Landsat bands as well as DVI, RVI, NDVI and EVI calculated from the Landsat data were iteratively entered into linear regressions against field-measured whole canopy %N.

2.3.3. MODIS

The spatial resolution of the MODIS reflectance (NBAR) product is 500 m—an area that would take more than 700 AVIRIS pixels to fill. This poses a challenge to comparison of MODIS reflectance against field measurements: whereas the ~20 × 20 m plot size of the field measurements for our sites fairly closely matches the pixel size of both AVIRIS and Landsat, it represents a small fraction of the area covered by a MODIS pixel. Moreover, because the field measurements in our study were spatially distributed, we only had from 1 to 4 field plots per MODIS pixel. Nevertheless, because the study sites were selected to represent relatively homogeneous areas (most sites were centered on a flux tower; see Table 1 and Section 2.2.3), we felt that some means of comparing MODIS reflectance with measured canopy %N would still be informative. We performed this comparison using two approaches. First, we compared MODIS reflectance directly with plot-level field data, acknowledging that this assumes MODIS pixels could be adequately characterized with the small number of available field plots. As a second approach, we calculated mean canopy %N values for entire MODIS pixels using predicted values from the "benchmark" AVIRIS PLS regression model. This approach effectively used AVIRIS as a spatial scaling tool for linking small plots to much larger pixels. We accomplished this by geolocating the 7 × 7 km MODIS NBAR subset within the AVIRIS %N map for each site, and extracting the AVIRIS mean %N for the center 500 m MODIS pixel. Reflectance from the seven MODIS reflectance bands as well as DVI, RVI, NDVI and EVI calculated from the MODIS data were iteratively included in linear regressions against whole canopy %N from the field plots, as well as against the mean AVIRIS-derived canopy %N value for the center pixel from each MODIS subset.

3. Results

3.1. AVIRIS

3.1.1. Spectral resolution

The multi-site PLS regression of field-measured, whole-canopy %N with AVIRIS reflectance at the nominal 10 nm spectral resolution (i.e., the benchmark model) resulted in a strong, highly significant relationship ($r^2 = 0.86$, PRESS RMSE = 0.21 and RMSE = 0.19; Table 3a, Fig. 1a) and produced a predicted versus observed trend that did not differ significantly from the 1:1 line. Predicted and observed %N values were lowest in evergreen-dominated forests, highest in deciduous forests and intermediate in mixed forests, although there was some degree of overlap and the trend was highly significant within as well as among forest types ($p < 0.0001$ for all forest types, individually and combined). When the PLS regression analysis was repeated using AVIRIS data sequentially degraded to 30 nm, 50 nm, 70 nm and 90 nm spectral bands, we obtained nearly identical results and observed only small declines in the strength of the resulting relationships (Table 3a).

The first PLS factor in all regressions, regardless of bandwidth, accounted for the greatest amount of variation in %N, and weighted the NIR region most heavily (Fig. 2a). In fact, regression coefficients across bands varied with magnitude of reflectance, such that spectral regions with high reflectance (e.g., the NIR) had the largest influence on the resulting models (Fig. 2b). This is not surprising, given the association between increasing NIR reflectance and increasing %N previously observed for closed canopy temperate and boreal forests (Ollinger et al., 2008) and corroborated for the forested sites in this study (Fig. 1b).

The influence of the NIR region was also observed in results of linear regression analyses. Regardless of bandwidth, the AVIRIS wavelength centered at ~889 nm was consistently the first band entered and retained in stepwise multiple regressions of all bands on %N (with a probability threshold of $p < 0.05$ to enter). Though the minimum BIC and PRESS statistics suggested that from five to nine additional wavelengths improved the regression model, a simple linear regression of NIR reflectance near 889 nm—even for a bandwidth as wide as 90 nm—was highly significant and explained the dominant fraction of %N variability (Table 3b, Fig. 1c). Consistent with the baseline PLS model results, the %N–NIR reflectance trend was significant within as well as among forest types, indicating that forest type alone does not explain its underlying basis.

Relationships between canopy %N and vegetation indices were generally weak, with the exception of DVI. Regardless of spectral resolution, RVI, NDVI and EVI were only weakly correlated with canopy %N, while DVI was strongly and positively related to %N (Table 3c). Given the strong absorbance of red light by closed-canopy forests, DVI—which is simply NIR reflectance minus red reflectance—is almost entirely driven by the influence of variation in the NIR.

3.1.2. Spatial resolution

The strength of the %N-reflectance relationship declined when AVIRIS pixels were degraded from 18 m to 30 m, but not from 30 m to 60 m (Table 3). Moreover, whereas spectral bandwidth had very little effect on the N-reflectance regression results with AVIRIS nominal pixel size (18 m), PLS results were significantly weaker for 30 m and 60 m pixel sizes when bandwidth was coarsened. The relationship between canopy %N and both NIR reflectance and the DVI for 30 m and 60 m data was weaker than for 18 m data, but little to no loss of prediction power was observed as bandwidth was coarsened (Table 3). These results are not surprising, given that the main advantage presented by PLS regression—e.g., the ability to produce robust equations even when the number of variables (i.e., bands) exceeds the number of field observations—is lost as bandwidth is degraded and the number of variables decreases. (See Table 3 for all regression results.)

3.1.3. AVIRIS simulations of Landsat and MODIS reflectance

There were no significant relationships between %N and reflectance from Landsat or MODIS visible bands as simulated with AVIRIS (Fig. 3a–c). However, reflectance from NIR and mid-IR bands was significantly related to %N (Fig. 3d–f). The most highly significant correlation with %N was from simulated Landsat and MODIS NIR bands centered at 830 nm and at 865 nm, respectively. Individually, these bands accounted for 79% (RMSE 0.25) and 80% (RMSE 0.24) of variation in %N, respectively (Table 4, Fig. 3d).

The regression results of vegetation indices calculated from AVIRIS simulations of Landsat and MODIS bands on canopy %N were similar to those calculated from nominal AVIRIS wavelengths, with weak relationships between %N and all vegetation indices except DVI, which yielded results similar to those of NIR reflectance alone (Table 4).

Table 3
Results from regression of AVIRIS spectral reflectance on whole canopy %N for all sites ($n = 155$), with progressively coarsened bandwidth and pixel size. (a) PLS regression of reflectance from all wavelengths on canopy %N; (b) simple linear regression (SLR) of reflectance from a single NIR band centered at 889 nm[a] on %N; (c) simple linear regression (SLR) of vegetation indices on canopy %N. Relationships were significant at $p < 0.0001$ unless otherwise noted.

	18 m (nominal pixel size)			30 m			60 m		
	PRESS RMSE[b]	r^2	RMSE[c]	PRESS RMSE[b]	r^2	RMSE[c]	PRESS RMSE[b]	r^2	RMSE[c]
(a) PLS (# factors)									
10 nm (5)	0.21	0.86	0.19	0.30	0.78	0.26	0.30	0.79	0.25
30 nm (4)	0.21	0.87	0.18	0.33	0.73	0.31	0.35	0.71	0.33
50 nm (3)	0.22	0.86	0.21	0.34	0.75	0.32	0.35	0.73	0.33
70 nm (3)	0.22	0.86	0.21	0.34	0.74	0.33	0.35	0.72	0.34
90 nm (3)	0.22	0.85	0.21	0.34	0.73	0.33	0.35	0.71	0.34
(b) SLR NIR									
10 nm	0.24	0.81	0.24	0.31	0.68	0.31	0.32	0.67	0.31
30 nm	0.24	0.81	0.24	0.31	0.68	0.31	0.32	0.65	0.32
50 nm	0.24	0.80	0.24	0.31	0.67	0.31	0.32	0.65	0.32
70 nm	0.25	0.80	0.24	0.32	0.67	0.31	0.33	0.64	0.32
90 nm	0.25	0.79	0.25	0.32	0.67	0.31	0.33	0.64	0.33
(c) SLR VI									
DVI									
10 nm	0.22	0.83	0.22	0.29	0.71	0.29	0.30	0.70	0.30
30 nm	0.23	0.83	0.22	0.29	0.71	0.29	0.31	0.68	0.31
50 nm	0.23	0.83	0.23	0.29	0.71	0.29	0.31	0.68	0.31
70 nm	0.23	0.82	0.23	0.30	0.71	0.29	0.31	0.68	0.31
90 nm	0.23	0.82	0.23	0.30	0.71	0.29	0.31	0.68	0.31
RVI									
10 nm	0.50	0.17	0.50	0.46	0.29	0.46	0.47	0.29	0.46
30 nm	0.48	0.23	0.48	0.45	0.34	0.44	0.49	0.24	0.48
50 nm	0.45	0.33	0.44	0.40	0.46	0.40	0.44	0.37	0.43
70 nm	0.41	0.44	0.41	0.37	0.54	0.37	0.40	0.48	0.40
90 nm	0.39	0.49	0.39	0.36	0.56	0.36	0.38	0.52	0.38
NDVI									
10 nm	0.49	0.20	0.49	0.48	0.24	0.47	0.48	0.24	0.48
30 nm	0.49	0.21	0.48	0.47	0.26	0.47	0.48	0.25	0.47
50 nm	0.47	0.25	0.47	0.46	0.30	0.46	0.46	0.29	0.46
70 nm	0.46	0.30	0.45	0.44	0.35	0.44	0.45	0.34	0.44
90 nm	0.44	0.34	0.44	0.43	0.39	0.42	0.43	0.38	0.43
EVI									
10 nm	0.52	0.08	0.52	ns	ns	ns	ns	ns	ns
30 nm	0.52	0.09	0.52	ns	ns	ns	ns	ns	ns
50 nm	0.51	0.13	0.51	ns	ns	ns	ns	ns	ns
70 nm	0.49	0.18	0.49	0.51	0.13	0.51	0.52	0.11	0.52
90 nm	0.48	0.23	0.48	0.50	0.16	0.50	0.51	0.15	0.51

[a] As determined through stepwise regression and corroborated with iterative simple linear regressions of reflectance at each wavelength on %N, reflectance at this individual wavelength alone explained more variability in %N than reflectance at any other wavelength, and was highly statistically significant for all bandwidths ($p < 0.0001$).
[b] PRESS RMSE = RMSE of residuals derived from iterative plot exclusion and prediction in model fitting.
[c] RMSE = error of calibration; quantifies the average difference between predicted v. measured %N.

3.2. Landsat

Regression results of actual Landsat reflectance on %N followed patterns similar to those from Landsat reflectance data simulated with AVIRIS, with no relationship observed between %N and the Landsat visible bands (Fig. 3a–c). However, whereas bands 4 (830 nm), 5 (1670 nm) and 7 (2240 nm) from AVIRIS-simulated Landsat data all were statistically significantly related to %N, here only bands 4 and 5 were correlated to %N. Moreover, while there was a significant, positive relationship between %N and Landsat band 4 ($r^2 = 0.53$, RMSE = 0.35), the relationship was much noisier than that observed with the AVIRIS-simulated band 4 ($r^2 = 0.79$, RMSE = 0.25; Table 4, Figs. 3d and 4).

Regression models with Landsat vegetation indices and %N were weaker than those from AVIRIS-simulated data, but the Landsat vegetation index with the most highly significant correlation with %N was still DVI ($r^2 = 0.61$, RMSE = 0.32; Table 4).

3.3. MODIS

The relationship between MODIS NIR reflectance and canopy %N was highly significant when using both the direct %N field measurements, and %N estimated for MODIS pixels using the baseline AVIRIS model (Table 4, Figs. 3d and 4). No significant relationships were observed between %N and either blue or green reflectance from MODIS (Fig. 3a–b), but a weak negative relationship was observed between %N and MODIS red reflectance ($r^2 = 0.25$, RMSE = 0.45, $p = 0.0085$; Fig. 3c).

Consistent with observations of %N and vegetation indices derived from AVIRIS and Landsat, relationships were more highly significant with MODIS-derived DVI than all other indices. However, regression results from MODIS-derived RVI on %N ($r^2 = 0.56$) were stronger than those derived from AVIRIS ($r^2 = 0.50$; Table 3) or Landsat ($r^2 = 0.05$; Table 4).

4. Discussion

The purpose of this study was to evaluate how observed relationships between spectral reflectance and forest canopy %N vary as a function of sensor properties, with the goals of furthering our understanding of factors affecting reflectance and advancing approaches to estimating spatial patterns in %N. As with any empirically based method of remote sensing, results should be applied only within the domain of the data used to generate them and not, for example, extended to tropical forests, non-forest biomes or heavily disturbed areas that lack closed canopies. Other approaches to %N mapping that can potentially be applied

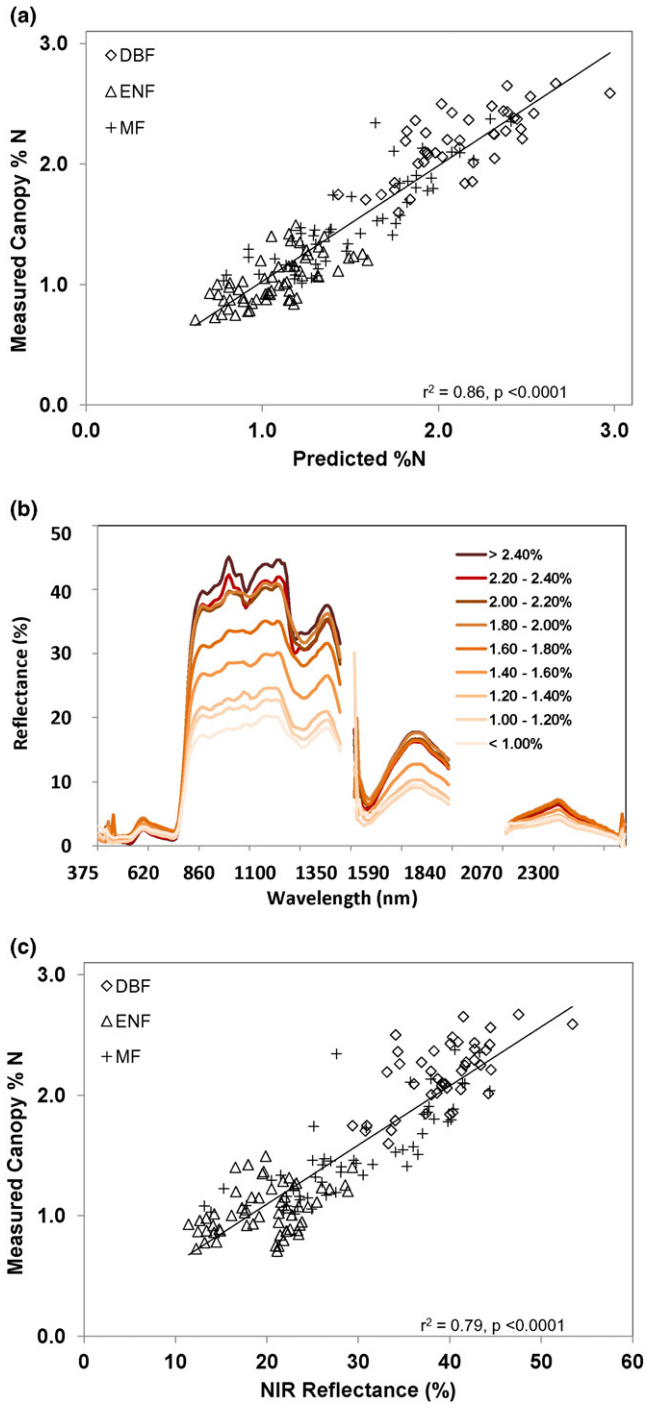

Fig. 1. Observed relationships between measured canopy %N and AVIRIS reflectance. In (a) measured %N is plotted against %N predicted with PLS regression of the full spectrum of AVIRIS data. Across the entire data set, the relationship is highly significant ($r^2 = 0.86$, $p < 0.0001$) with a low standard error of calibration (0.19). Predicted r^2 is also significant within each forest type: DBF $r^2 = 0.54$; ENF $r^2 = 0.36$; MF $r^2 = 0.74$; $p < 0.0001$ for each. PLS factor loadings were most influenced by NIR bands, and likely reflect the pattern of increasing NIR reflectance with increasing %N observed in (b), where average AVIRIS spectra were plotted for our study sites grouped into 9 classes of %N. Specifically, %N values for all sites in our study were grouped into ranges of %N, binned incrementally by 0.20. AVIRIS reflectance values for all sites within each foliar N bin were averaged, and these average reflectance values were plotted. The influence of the NIR region is further demonstrated in (c), where AVIRIS reflectance was averaged over the wavelengths from ~850 to 930 nm and entered into a simple linear regression on %N for all our study sites. Although the relationship between %N and this one 90 nm-wide band contains more scatter (RMSE = 0.25), it remained significant ($p < 0.0001$) across all forest types ($r^2 = 0.79$, $p < 0001$) as well as within each forest type individually: DBF $r^2 = 0.40$; ENF $r^2 = 0.19$; MF $r^2 = 0.66$; $p < 0.001$ for each. See Table 3 for further details on simple linear regression of %N and NIR reflectance.

more generally include inversion of radiative transfer models that predict reflectance properties based on understanding mechanisms through which photons interact with plants (e.g., Asner, Wessman, Schimel, & Archer, 1998; Peddle, Johnson, Cihlar, & Latifovic, 2004; Zhang et al., 2006). However, because N in plants is present in a variety of compounds, many of which lack distinct spectral signatures, mechanistic approaches to N detection are extremely challenging. Hence, as with applications of remote sensing to a wide variety of vegetation properties, empirical approaches continue to offer a useful path forward. While this approach is not without its limitations, expanding our knowledge of associations between %N and canopy reflectance—where they apply, where they break down, and how they vary with sensor characteristics—can provide useful insights and highlight future research needs.

4.1. Sensor properties

All regression models with AVIRIS reflectance data on canopy %N were more robust than those with Landsat or MODIS data. Correlations between reflectance and %N showed relatively little decline when AVIRIS wavelengths were coarsened to as wide as 90 nm (Table 3, Fig. 1c). Additionally, correlations of %N with MODIS reflectance were stronger than those with Landsat reflectance (Table 4); this is notable, given that MODIS pixels are more than 16 times larger than Landsat pixels. These results suggest that neither bandwidth nor pixel size alone can fully explain the differences in observed %N-reflectance relationships and suggest an additional effect, possibly related to sensor fidelity.

The design of the AVIRIS instrument and continual improvements to its optics have advanced this sensor's data quality up to an order of magnitude over that from other existing sensors. In particular, the SNR of AVIRIS can be more than ten times higher than that of Landsat and nearly four times higher than MODIS (see Table 2). With 16-bit quantization, AVIRIS imagery also represents a larger dynamic range than Landsat 5 and MODIS imagery. These factors undoubtedly contributed to the stronger N-reflectance relationships with AVIRIS than with Landsat and MODIS spectral data, and support observations reported elsewhere (Elmore & Mustard, 2003; Goodenough et al., 2003). These observations also bode well for Landsat 8, whose Operational Land Imager (OLI) has higher SNR than Landsat 5 and 7 and 12-bit quantization (Irons, Dwyer, & Barsi, 2012; Roy et al., 2014).

Results from regressions of MODIS NIR reflectance on %N were surprisingly strong, especially given the 500 m MODIS pixel size (Table 4). Again, this may stem from the combination of MODIS 12-bit quantization (vs. 8-bit Landsat 5 quantization) and SNR up to four times higher than Landsat 5. Moreover, the fact that the MODIS reflectance product has been BRDF-corrected extends the potential utility of MODIS to a larger range of sun-angle and topographic conditions than aircraft sensor data that are not routinely BRDF-corrected. As an example, regression results of MODIS reflectance on AVIRIS-derived canopy %N when all 196 pixels in the 7 × 7 km MODIS subset image were included were far weaker ($r^2 = 0.55$, RMSE = 0.33) than when only the center MODIS pixel was included ($r^2 = 0.77$, RMSE = .25). This is not surprising, given that the center MODIS pixel for all sites in this study (with the exception of the Catskills) is centered on an eddy covariance tower site that generally represent more homogeneous areas than those contained within the wider MODIS subset images. Moreover, MODIS reflectance data were related to %N data derived from AVIRIS that are not BRDF-corrected. The AVIRIS flightlines for the sites in this analysis were centered over the eddy flux towers—i.e., the center of a North–South AVIRIS flightline was nadir-pointing. With a scan angle of 15° off-nadir, AVIRIS pixels could be slightly distorted at the edge of the scan lines (Fischer & Ryan, 2002). For this reason, comparisons of MODIS NBAR data to AVIRIS off-nadir data may include brightness effects resulting from differences in sun and sensor angle exacerbated by topography over heterogeneous landscapes.

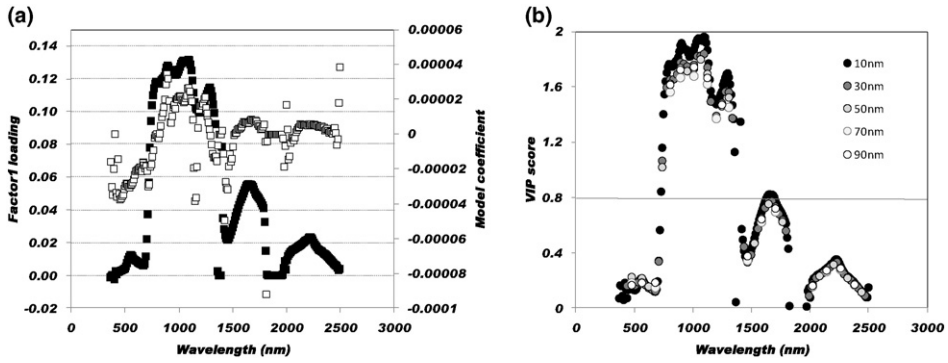

Fig. 2. Factor loadings and full PLS model coefficients for PLS regression of AVIRIS spectra on canopy %N (a). Patterns of loadings and coefficients were the same regardless of spectral resolution, but panel (a) includes results from the original 10 nm data only, for simplicity. Solid symbols in (a) represent loadings; open symbols represent model coefficients. Variable importance for projection (VIP) scores are shown in panel (b) for all spectral bandwidths examined here. The VIP score is a measure of each wavelength's importance in the model, with values less than 0.80 exerting little influence on the regression model. These figures highlight the influence of NIR reflectance in our regression models for estimating N concentration.

Collectively, our results indicate that the potential to estimate canopy %N for pixels as coarse as 500 m with a simple regression model may be most limited not by sensor fidelity, but by lack of field measurements for an area this size, and by insufficient understanding of how the %N–NIR relationship may vary over the full range of conditions contained within large MODIS scenes.

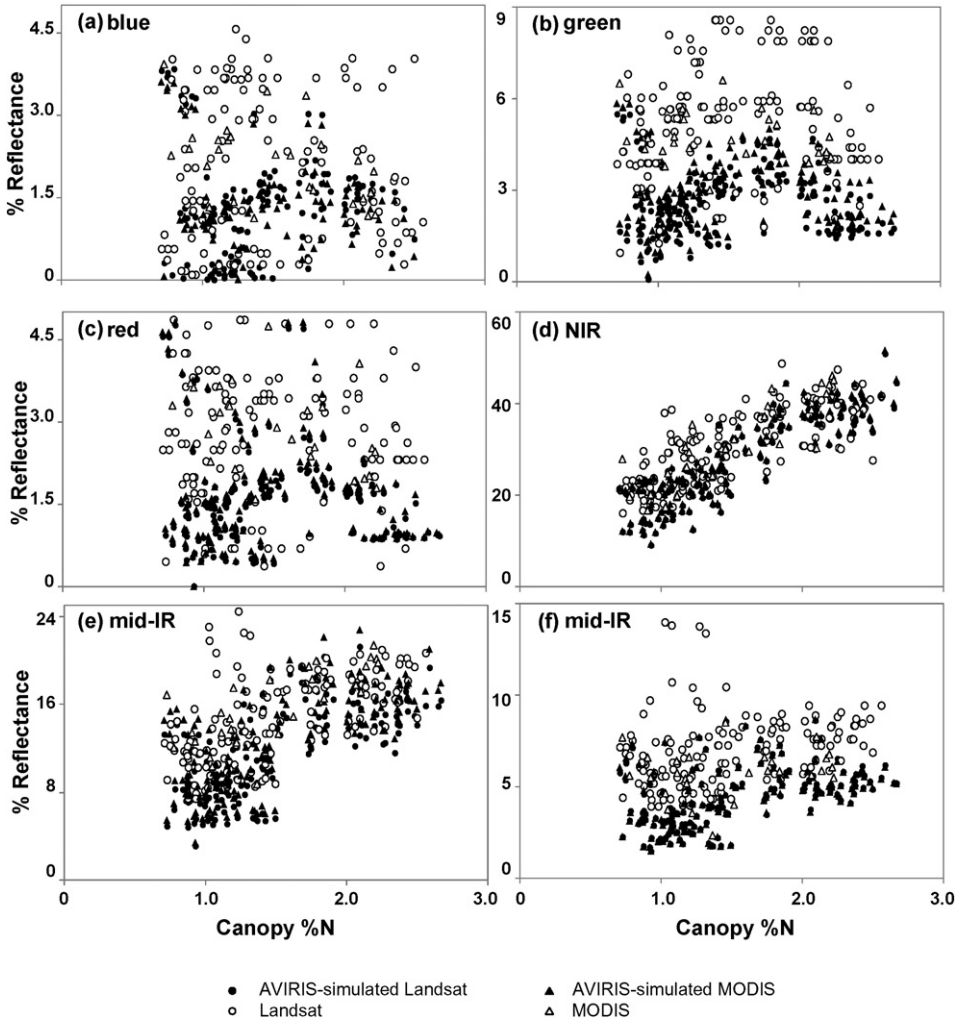

Fig. 3. Observed relationships between canopy %N and reflectance at Landsat and MODIS band centers. Solid symbols represent AVIRIS simulations of Landsat and MODIS reflectance; open symbols represent actual Landsat and MODIS reflectance. No significant relationships were observed between %N and visible reflectance (a–c). A weak negative relationship was observed between %N and actual MODIS red reflectance ($r^2 = 0.25$, RMSE = 0.45, $p = 0.0085$) (c). Highly significant relationships ($p < 0.0001$) were observed between %N and reflectance at the NIR band (d) for all data (simulated and actual), and weak correlations with the mid-IR bands (e–f). These observations illustrate why vegetation indices that represent some combination of NIR bands and visible bands in regression equations do not tend to explain more variability in %N than NIR alone (see Table 4). Rather, the visible bands appear to add noise to an otherwise strong correlation between %N and NIR reflectance. (See Table 2 for spectral ranges.)

Table 4
Regression statistics from analyses of canopy %N with reflectance at Landsat and MODIS spectral bands, as simulated with AVIRIS and as obtained directly from Landsat and MODIS sensors.

Sensor	Spectral band or vegetation index	Simulated		Actual	
		r^2	RMSE (PRESS)	r^2	RMSE (PRESS)
Landsat	NIR band (830 nm)	0.79	0.25 (0.25)	0.53	0.35 (0.36)
	DVI	0.82	0.23 (0.23)	0.61	0.32 (0.32)
	RVI	0.36	0.43 (0.44)	0.05	0.50 (0.50)
	NDVI	0.23	0.48 (0.48)	0.13	0.48 (0.48)
	EVI	0.05	0.53 (0.53)	0.07	0.49 (0.49)
MODIS[a]	NIR band (865 nm)	0.80	0.24 (0.25)	0.80^{P}	$0.30\ (0.30)^{P}$
				0.77^{A}	$0.25\ (0.25)^{A}$
	DVI	0.82	0.23 (0.23)	0.81^{P}	$0.29\ (0.29)^{P}$
				0.79^{A}	$0.24\ (0.24)^{A}$
	RVI	0.40	0.42 (0.43)	0.56^{P}	$0.44\ (0.44)^{P}$
				0.65^{A}	$0.30\ (0.30)^{A}$
	NDVI	0.26	0.47 (0.47)	0.49^{P}	$0.47\ (0.48)^{P}$
				0.53^{A}	$0.35\ (0.37)^{A}$
	EVI	0.12	0.51 (0.51)	0.34^{P}	$0.54\ (0.55)^{P}$
				0.34^{A}	$0.42\ (0.43)^{A}$

All regressions are significant at the 95% confidence level.
[a] Statistics for simulated MODIS data represent 18 m AVIRIS reflectance at nominal spatial resolution (18 m) resampled to MODIS bandwidth and band centers, and analyzed with plot-level %N. Because of the mismatch between field plot size (20 m) and MODIS pixel size (500 m), statistics for actual MODIS data represent results from MODIS reflectance (500 m) analyzed against (^{P}) plot-level %N as well as against (^{A}) mean %N for the entire 500 m area, derived from averaging N values from the benchmark AVIRIS model for all AVIRIS pixels that intersect the 500 m MODIS pixel (see Section 2.3.3).

4.2. Vegetation indices, NIR and visible reflectance

The vegetation index most strongly correlated with canopy %N was DVI—the simplest of all indices included in our analysis. In fact, correlations with %N appeared to decline as indices became more complex, with NDVI and EVI most weakly correlated with canopy %N (e.g., Tables 3–4). These results indicate that the relationship between %N and the indices in our analysis were driven more so by variation in NIR reflectance than by variation in visible reflectance. This observation supports the notion that the contribution of visible reflectance in some vegetation indices can add noise to an otherwise strong correlation between NIR reflectance and %N (e.g., Kruse et al., 2006; Ollinger, 2011), though the mechanism behind the correlation is not fully understood.

A plausible explanation for the %N–NIR relationship is that %N covaries with canopy structural properties, such as LAI, that influence reflectance. However, given that the vegetation indices included in this study are often used for estimating biomass and LAI, the lack of a strong correlation between the indices and %N suggest that neither of these variables alone is driving the %N–NIR relationship. Moreover, when %N was compared to the limited plot-level LAI measurements available in our dataset (e.g., Fig. 5a), no relationship between LAI and %N was observed. This supports previous work by Ollinger et al. (2008), who also observed no relationship between measured LAI and either albedo (e.g., total shortwave reflectance) or canopy %N (Fig. 5b). This does not mean that other attributes of canopy structure are unimportant (see Section 4.3) and it should be kept in mind that our dataset is limited to closed-canopy forests. In systems with sparse canopies, low stem density, or lower LAI, vegetation indices that include reflectance from visible wavelengths may aid in the interpretation of the NIR signal. Nevertheless, here no significant relationships were observed between %N and reflectance in the visible wavelengths, with the exception of MODIS red reflectance. There are a few possible explanations for this. First, whereas AVIRIS and Landsat data here represent reflectance for one day during the growing season, MODIS data represent composites from a 16-day period. As a result, MODIS data potentially spanned a larger range of variability in reflectance than did AVIRIS or Landsat. Second, the MODIS reflectance data product is corrected using the BRDF to integrate scattering at all view angles (Schaaf et al., 2002); AVIRIS and Landsat data were transformed from radiance to reflectance, but represent only one view angle. Together, these factors may have contributed to a weak but statistically significant pattern of decreasing MODIS red reflectance with increasing MODIS NIR reflectance, and, as a result, MODIS was the only data set in our comparisons where RVI was strongly related to %N.

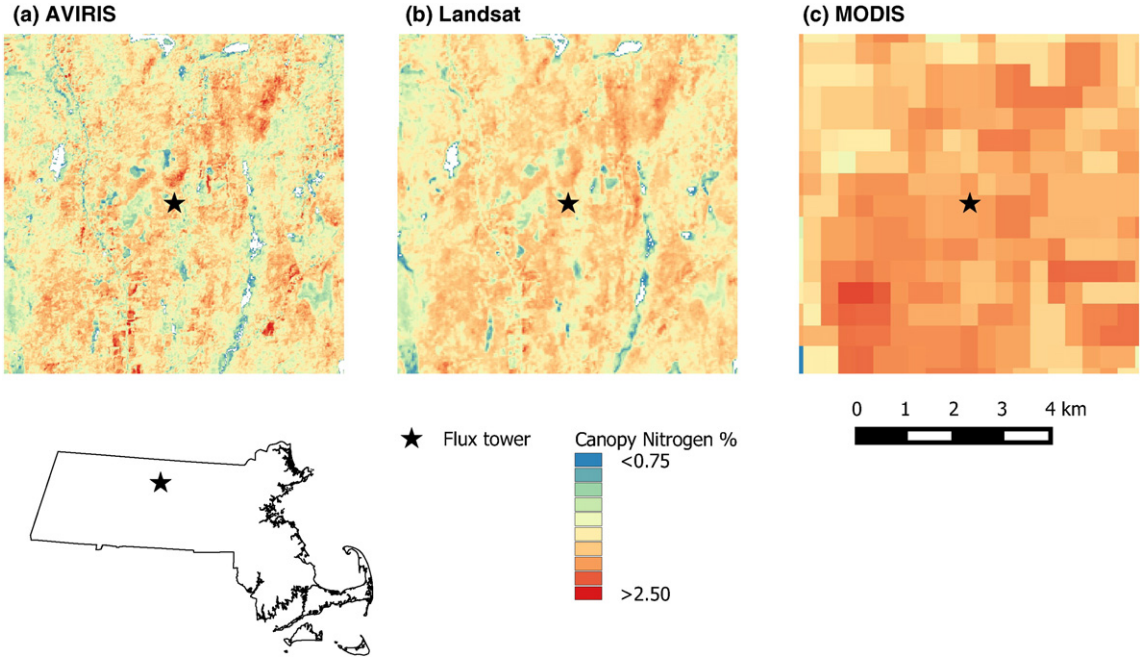

Fig. 4. A sample comparison of canopy %N spatial patterns shown for a 7 × 7 km area around the Harvard Forest flux tower site in Massachusetts, USA (see Table 1). Predictions are derived from (a) AVIRIS, using a simple linear regression of field %N and AVIRIS reflectance from one NIR wavelength; (b) Landsat 5, using a simple linear regression of field %N and NIR reflectance (band 4); and (c) MODIS, using a simple linear regression of field %N and MODIS NIR reflectance (NBAR band 2). Prediction models and statistics are given in Tables 3b and 4.

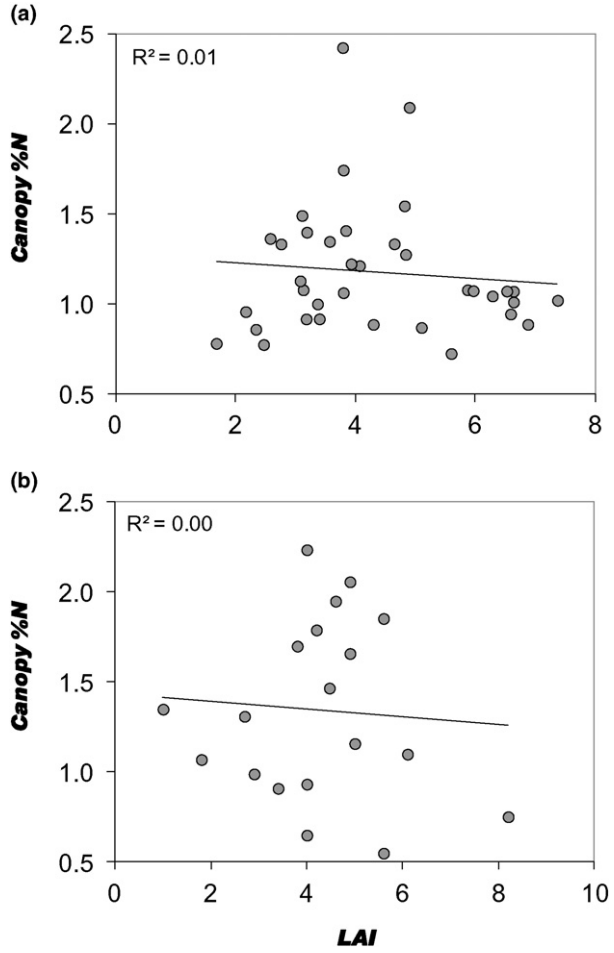

Fig. 5. Canopy %N in relation to LAI. The top panel (a) represents LAI as measured at 36 of the 155 plots from the existing dataset on which this analysis was based. The bottom panel (b) represents canopy %N and LAI for a 250 m radius footprint around flux tower sites from the U.S. and Canada, as reported in Ollinger et al. 2008. In both cases, no relationship was observed between %N and LAI.

4.3. Underlying basis for estimating canopy %N

Much of the effort on detection of %N and other biochemical constituents in plants has involved development of empirical prediction models (e.g., Coops et al., 2003; Martin et al., 2008; McNeil et al., 2008; Townsend et al., 2003; Wessman et al., 1988). This does not, however, mean the results lack biological underpinnings. Because nitrogen availability is among the most important constraints on photosynthesis, evolution selects for individuals that optimize its use, particularly with respect to investments in light harvesting and acquisition of other limiting resources. As a result, N concentrations in foliage are directly or indirectly coupled with a broad suite of plant traits that range from biochemical composition (e.g., Evans, 1989) to leaf shape (e.g., Niinemets, Cescatti, Lukjanova, Tobias, & Truus, 2002) and crown structure (e.g., Cohen & Pastor, 1996). Although these associations are complex and not thoroughly understood, they can be grouped into those having direct versus indirect effects on reflectance. Direct effects involve the role of N in pigments and other compounds that interact with photons directly (e.g., Daughtry, Walthall, Kim, de Colstoun, & McMurtrey, 2000; Kokaly et al., 2009), while indirect effects involve associations between leaf %N, C assimilation and plant structural features that affect scattering and light harvesting (e.g., Ollinger, 2011).

At leaf and stem levels, for instance, indirect effects involve traits that have been observed to vary with foliar %N or photosynthetic capacity—such as cellular leaf anatomy (Hollinger et al., 2010; Longstreth, Bolaños, & Goddard, 1985; Slaton, Hunt, & Smith, 2001), leaf clumping (Niinemets et al., 2002) and leaf angle distribution (Close & Beadle, 2006; Hollinger, 1996; King, 1997; Posada, Lechowicz, & Kitajima, 2009; Valiente-Banuet, Verdú, Valladares, & García-Fayos, 2010)—that also affect scattering and reflectance in the NIR region. In addition to leaf- and stem-level factors, evidence suggests a role of N status at the whole tree and canopy scale that may influence crown geometry, and hence NIR reflectance (Ollinger, 2011). For example, forests with low resource availability tend to have lower ratios of allocation to wood relative to foliage (e.g. Litton, Raich, & Ryan, 2007), which should result in narrower, more conical tree crowns (Cohen & Pastor, 1996) and lower reflectance across the NIR region (e.g. Rautiainen, Mõttus, Stenberg, & Ervasti, 2008).

Our findings are among a growing number of studies that have observed strong relationships between canopy %N and NIR reflectance (Goel et al., 2003; Kruse et al., 2006; Ollinger et al., 2008; Nigon et al., 2012; Serrano, Filella, & Peñuelas, 2000). Given that the NIR region is typically indicative of structural features that influence scattering, rather than biochemically driven absorption features, this underscores the importance of indirect effects of plant traits on reflectance. Nevertheless, we note that PLS regression with full spectrum, narrowband data yielded the strongest results in our analysis, possibly because it capitalizes on both direct effects of N on plant spectra (e.g. spectral absorption features) and the indirect effects of associations that affect light scattering.

4.4. Implications for future work

Given that we observed no effect of bandwidth on the strength of the relationship between %N and canopy reflectance, a possible conclusion is that the hundreds of narrow wavelengths in imaging spectrometers are superfluous. However, our analysis represents only closed-canopy forests in North America, and involves estimation of only one biochemical constituent. Hence, advocating only for broad-band features in future Earth observing sensors would be premature and potentially short-sighted. A high-fidelity sensor with a large number of bands could stand to benefit ecological applications that require sensitivity to vegetation spectral properties, such as identification of specific macronutrients and other compounds (e.g., Cho, van Aardt, Main, & Majeke, 2010; Gil-Pérez et al., 2010; Pacumbaba & Beyl, 2011); estimation of leaf water content (e.g., Wang, Xu, & Yang, 2009; Zygielbaum, Gitelson, Arkebauer, & Rundquist, 2009); plant species discrimination (e.g., Clark, Roberts, & Clark, 2005; Cochrane, 2000; Dennison & Roberts, 2003; Plourde, Ollinger, Smith, & Martin, 2007; Pu, 2009); detection of plant stress (Pontius, Hallett, & Martin, 2005; Suárez et al., 2008) or non-native species (Hestir et al., 2008; Underwood et al., 2006); and estimation of total shortwave albedo (e.g., Molotch & Bales, 2006; Roberts et al., 2004) to name just a few. Further, whereas the finest spatial resolution included in our analysis was 18 m, studies conducted at finer scales, potentially examining properties of individual plants, or open canopy ecosystems that include reflectance by underlying substrate, may benefit from narrow-band, full spectrum data in ways that our study was not intended to evaluate.

Moreover, in the absence of a more detailed understanding of the NIR–%N relationship, our ability to apply it is currently limited to the forest types and environmental conditions represented in the data. Future work in narrowband spectroscopy—e.g., determining the individual and combined effects on narrowband spectra of canopy architecture, leaf angle distribution, crown geometry, and foliar chemistry—may shed additional light on the mechanisms that drive the N–NIR relationship, and how it will be affected by changes in climate, nitrogen deposition, or other forms of disturbance.

Data from planned satellite-based Earth observation missions such as the HyspIRI imaging spectrometer and the National Ecological Observatory Network (NEON; Kampe, Johnson, Kuester, & Keller, 2010) in the U.S. also stand to advance both our understanding of relationships

between plant chemistry and spectral properties, and methods for N mapping across broad scales. HyspIRI will provide the first global coverage of vegetation spectral properties at radiometric and spectral resolutions comparable to those of AVIRIS. Coupled with detailed field and aircraft data collected as part of NEON, these data will allow for refinement of N-mapping methods over a wide range of biomes, while enabling continued progress toward a better understanding of reflectance–N relationships under contemporary and future conditions.

Our results nevertheless suggest new applications for broad-band sensor data under contemporary conditions that have relevance to regional modeling efforts. For instance, while our results demonstrate that forest composition alone does not explain all variability in NIR reflectance (e.g., Section 3.1.1), because the N–NIR relationship incorporates structural and biophysical parameters that are most apparent in NIR reflectance it allows for accurate estimation of forest composition across broad scales (e.g., Fig. 1). The ability to determine the proportion of deciduous and coniferous components of forests would stand to improve both parameterization of and predictions from models that rely on accurate proportions of forest type to examine ecosystem processes at broad scales.

5. Conclusions

Results from regressions of AVIRIS reflectance on canopy N from 13 forested sites in North America suggest that general methods for %N estimation over broad spatial scales should be possible with future high-fidelity global imaging spectrometers as well as high-fidelity broad-band sensors. We saw little loss of accuracy when AVIRIS spectra were degraded to coarse bandwidths, suggesting that some of the synergy captured with narrowband data is also captured by broad-band sensors. The strength of relationships between measured canopy %N and simple measures of NIR reflectance from MODIS and Landsat—even with coarse pixel resolution—indeed suggests that existing broad-band sensors may already have value for estimating %N. Nonetheless, relationships between measured %N and NIR reflectance from Landsat and MODIS were weaker than those using AVIRIS data aggregated to Landsat and MODIS spectral resolutions. This suggests that the benefit of AVIRIS data for canopy %N estimation may lie in its higher data quality rather than its finer spectral and spatial resolution.

Full-spectrum PLS regression of narrowband imaging spectrometer data may remain the most accurate method for estimating canopy %N. In the absence of narrowband data, however, broad-band multispectral data may yet provide acceptable estimates of %N, particularly over larger areas, and may help inform future research and sensor development related to studies of vegetation and environmental change.

Given future Earth observation missions that include plans for a satellite-based, fine-resolution imaging spectrometer, results reported here nevertheless indicate promise for the possibility of broad-scale N mapping. Our ability to predict conditions under future change scenarios, however, is limited to contemporary conditions because the mechanistic driver in the link between NIR reflectance and canopy N remains unclear. For this reason, future research in this area should involve refinement of N-mapping methods to include a broad range of ecosystems and land cover types as well as further experimentation to better understand the extent to which changes in plant N status, N availability, or increases in N or other atmospheric inputs, will also change NIR reflectance.

Acknowledgments

Funding and AVIRIS data were provided by NASA in support of the following grants: NASA Carbon Cycle Science Award #NNX08AG14G and #NNX14AJ18G, and NASA Terrestrial Ecology Award #NNX11AB88G. Portions of this research were also supported through the Harvard Forest and Hubbard Brook Long Term Ecological Research programs (NSF 1237491 and 1114804, respectively) and the USDA Forest Service, Northeastern States Research Cooperative (Award #15-DG-11242307-053). We also acknowledge the Canadian Carbon Program, and the following individuals for their valuable insight as well as assistance with sample collection: Alan Barr, Nicholas Coops, Michelle Day, Steve Frolking, Thomas Hilker, Hank Margolis, Jean-Lionel Payeur-Poirier, Christophe Rouyer, and Erin Thompson. We are also indebted to the individuals who provided reviews of this manuscript, and whose suggestions contributed to a substantially improved paper.

References

Aber, J.D. (1979a). Foliage-height profiles and succession in northern hardwood forests. *Ecology*, *60*, 18–23. http://dx.doi.org/10.2307/1936462.

Aber, J.D. (1979b). A method for estimating foliage-height profiles in broad-leaved forests. *Journal of Ecology*, *67*, 35–40. http://dx.doi.org/10.2307/2259335.

Asner, G.P., & Vitousek, P.M. (2005). Remote analysis of biological invasion and biogeochemical change. *Proceedings of the National Academy of Sciences of the USA*, *102*, 4383–4386. http://dx.doi.org/10.1073/pnas.0500823102.

Asner, G.P., Knapp, D.E., Kennedy-Bowdoin, T., Jones, M.O., Martin, R.E., Boardman, J., & Field, C.B. (2007). Carnegie Airborne Observatory: In-flight fusion of hyperspectral imaging and waveform light detection and ranging (wLIDAR) for three-dimensional studies of ecosystems. *Journal of Applied Remote Sensing*, *1*(013536), 1–21. http://dx.doi.org/10.1117/1.2794018.

Asner, G.P., Wessman, C.A., Schimel, D.S., & Archer, S. (1998). Variability in leaf and litter optical properties: Implications for BRDF model inversions using AVHRR, MODIS and MISR. *Remote Sensing of Environment*, *63*, 243–257. http://dx.doi.org/10.1016/S0034-4257(97)00138-7.

Bolster, K.L., Martin, M.E., & Aber, J.D. (1996). Determination of carbon fraction and nitrogen concentration in tree foliage by near infrared reflectance: A comparison of statistical methods. *Canadian Journal of Forest Research*, *26*(4), 590–600. http://dx.doi.org/10.1139/x26-068.

Chen, Y., Ji, Y., Zhou, J., Chen, X., & Shen, W. (2012). Computation of signal-to-noise ratio of airborne hyperspectral imaging spectrometer. *2012 International conference on systems and informatics* (pp. 1046–1049). http://dx.doi.org/10.1109/ICSAI.2012.6223191.

Chien, S., Silverman, D., Davies, A.G., & Mandl, D. (2009). Onboard science processing concepts for the HyspIRI mission. *IEEE Intelligent Systems*, *24*(6), 12–19. http://dx.doi.org/10.1109/MIS.2009.120.

Cho, M.A., van Aardt, J., Main, R., & Majeke, B. (2010). Evaluating variations of physiology-based hyperspectral features along a soil water gradient in a *Eucalyptus grandis* plantation. *International Journal of Remote Sensing*, *31*, 3143–3159. http://dx.doi.org/10.1080/01431160903154390.

Clark, M.L., Roberts, D.A., & Clark, D.B. (2005). Hyperspectral discrimination of tropical rain forest tree species at leaf to crown scales. *Remote Sensing of Environment*, *96*, 375–398. http://dx.doi.org/10.1016/j.rse.2005.03.009.

Close, D.C., & Beadle, C.L. (2006). Leaf angle responds to nitrogen supply in eucalypt seedlings. Is it a photoprotective mechanism? *Tree Physiology*, *26*, 743–748.

Cochrane, M.A. (2000). Using vegetation reflectance variability for species level classification of hyperspectral data. *International Journal of Remote Sensing*, *21*, 2075–2087. http://dx.doi.org/10.1080/01431160050021303.

Cohen, Y., & Pastor, J. (1996). Interactions among nitrogen, carbon, plant shape, and photosynthesis. *The American Naturalist*, *147*, 847–865.

Coops, N.C., Smith, M. -L., Martin, M.E., & Ollinger, S.V. (2003). Prediction of eucalypt foliage nitrogen content from satellite-derived hyperspectral data. *IEEE Transactions on Geoscience and Remote Sensing*, *41*, 1338–1346. http://dx.doi.org/10.1109/TGRS.2003.813135.

National Research Council. (2007). Earth science and applications from space: National imperatives for the next decade and beyond. Committee on earth science and applications from space: A community assessment and strategy for the future. Washington, DC: The National Academies Press. (456 pp.)

Curran, P.J. (1989). Remote sensing of foliar chemistry. *Remote Sensing of Environment*, *30*, 271–278. http://dx.doi.org/10.1016/0034-4257(89)90069-2.

Curran, P.J., Kupiec, J. A., & Smith, G. M. (1997). Remote sensing the biochemical composition of a slash pine canopy. *IEEE Transactions on Geoscience and Remote Sensing*, *35*, 415–420. http://dx.doi.org/10.1109/36.563280.

Daughtry, C.S.T., Walthall, C.L., Kim, M.S., de Colstoun, E.B., & McMurtrey, J.E. (2000). Estimating corn leaf chlorophyll concentration from leaf and canopy reflectance. *Remote Sensing of Environment*, *74*(2), 229–239. http://dx.doi.org/10.1016/S0034-4257(00)00113-9.

Dennison, P.E., & Roberts, D.A. (2003). Endmember selection for multiple endmember spectral mixture analysis using endmember average RMSE. *Remote Sensing of Environment*, *87*, 123–135. http://dx.doi.org/10.1016/S0034-4257(03)00135-4.

Elmore, A.J., & Mustard, J.F. (2003). Precision and accuracy of EO-1 Advanced Land Imager (ALI) data for semiarid vegetation studies. *IEEE Transactions on Geoscience and Remote Sensing*, *41*, 1311–1320. http://dx.doi.org/10.1109/TGRS.2003.813132.

Evans, J.R. (1989). Photosynthesis and nitrogen relationships in leaves of C_3 plants. *Oecologia*, *78*, 9–19. http://dx.doi.org/10.1007/BF00377192.

Ferwerda, J., Skidmore, A.K., & Mutanga, O. (2005). Nitrogen detection with hyperspectral normalized ratio indices across multiple plant species. *International Journal of Remote Sensing*, *26*(18), 4083–4095. http://dx.doi.org/10.1080/01431160500181044.

Field, C., & Mooney, H.A. (1986). The photosynthesis-nitrogen relationship in wild plants. In T.J. Givnish (Ed.), *Proceedings of the sixth Maria Moors Cabot symposium, evolutionary constraints on primary productivity: Adaptive patterns of energy capture in plants, Harvard forest, August 1983* (pp. 25–55). Cambridge, UK: Cambridge University Press.

Fischer, A., & Ryan, J.P. (2002). Adapting the use of hyperspectral imagery in ocean process studies. *Monterey Bay Aquarium Research Institute Papers* (http://www.mbari.org/education/internship/02interns/02papers/andy.pdf).

Galloway, J.N., Aber, J.D., Erisman, J.W., Seitzinger, S.P., Howarth, R.W., Cowling, E.B., & Cosby, B.J. (2003). The nitrogen cascade. *Bioscience*, *53*(4), 341–356. http://dx.doi.org/10.1641/0006-3568(2003)053[0341:TNC]2.0.CO;2.

Gamon, J.A., Field, C.B., Goulden, M.L., Griffin, K.L., Hartley, A.E., Joel, G., ... Valentini, R. (1995). Relationships between NDVI, canopy structure and photosynthesis in three Californian vegetation types. *Ecological Applications*, *5*, 28–41. http://dx.doi.org/10.2307/1942049.

Geological Survey, U.S. (2011). Earth Resources Observation and Science (EROS) Center. http://eros.usgs.gov/#/Find_Data/Products_and_Data_Available/TM (Accessed April 19, 2011)

Gil-Pérez, B., Zarco-Tejada, P.J., Correa-Guimaraes, A., Relea-Gangas, E., Navas-Gracia, L.M., Hernández-Navarro, S., ... Martín-Gil, J. (2010). Remote sensing detection of nutrient uptake in vineyards using narrow-band hyperspectral imagery. *Vitis*, *49*, 167–173 (http://www.vitis-vea.de/admin/volltext/W0%2010%203178.pdf).

Goel, P.K., Prasher, S.O., Landry, L.A., Patel, R.M., Bonnell, R.B., Viau, A.A., & Miller, J.A. (2003). Potential of airborne hyperspectral remote sensing to detect nitrogen deficiency and weed infestation in corn. *Computers and Electronics in Agriculture*, *38*(2), 99–124. http://dx.doi.org/10.1016/S0168-1699(02)00138-2.

Goodenough, D.G., Dyk, A., Niemann, O., Pearlman, J.S., Chen, H., Han, T., ... West, C. (2003). Processing Hyperion and ALI for forest classification. *IEEE Transactions on Geoscience and Remote Sensing*, *41*, 1321–1331. http://dx.doi.org/10.1109/TGRS.2003.813214.

Green, D.S., Erickson, J.E., & Kruger, E.L. (2003). Foliar morphology and canopy nitrogen as predictors of light-use efficiency in terrestrial vegetation. *Agricultural and Forest Meteorology*, *115*, 163–171. http://dx.doi.org/10.1016/S0168-1923(02)00210-1.

Green, R.O. (2005). Updates to the AVIRIS calibration algorithm associated with the new AVIRIS fore optics. *Proceedings of the 14th JPL airborne geoscience workshop*. Pasadena, CA: Jet Propulsion Laboratory.

Green, R.O., Eastwood, M.L., Sarture, C.M., Chrien, T.G., Aronsson, M., Chippendale, B.J., ... Williams, O. (1998). Imaging spectroscopy and the Airborne Visible/Infrared Imaging Spectrometer (AVIRIS). *Remote Sensing of Environment*, *65*, 227–248. http://dx.doi.org/10.1016/S0034-4257(98)00064-9.

Helder, D.L., Ruggles, T.A., Dewald, J.D., & Madhavan, S. (2004). Landsat-5 Thematic Mapper reflective-band radiometric stability. *IEEE Transactions on Geoscience and Remote Sensing*, *42*, 2730–2746. http://dx.doi.org/10.1109/TGRS.2004.839088.

Hestir, E.L., Khanna, S., Andrew, M.E., Santos, M.J., Viers, J.H., Greenberg, J.A., ... Ustin, S.L. (2008). Identification of invasive vegetation using hyperspectral remote sensing in the California Delta ecosystem. *Remote Sensing of Environment*, *112*, 4034–4047. http://dx.doi.org/10.1016/j.rse.2008.01.022.

Hollinger, D.Y. (1996). Optimality and nitrogen allocation in a tree canopy. *Tree Physiology*, *16*, 627–634.

Hollinger, D.Y., Ollinger, S.V., Richardson, A.D., Meyers, T.P., Dail, D.B., Martin, M.E., ... Verma, S.B. (2010). Albedo estimates for land surface models and support for a new paradigm based on foliage nitrogen concentration. *Global Change Biology*, *16*, 696–710. http://dx.doi.org/10.1111/j.1365-2486.2009.02028.x.

Irons, J.R., Dwyer, J.L., & Barsi, J.A. (2012). The next Landsat satellite: The Landsat Data Continuity Mission. *Remote Sensing of Environment*, *122*, 11–21. http://dx.doi.org/10.1016/j.rse.2011.08.026.

Jandl, R., Lindner, M., Vesterdal, L., Bauwens, B., Baritz, R., Hagedorn, F., ... Byrne, K.A. (2007). How strongly can forest management influence soil carbon sequestration. *Geoderma*, *137*, 253–268. http://dx.doi.org/10.1016/j.geoderma.2006.09.003.

Jefferies, R.L., Klein, D.R., & Shaver, G.R. (1994). Vertebrate herbivores and northern plant-communities: Reciprocal influences and responses. *Oikos*, *71*, 193–206. http://dx.doi.org/10.2307/3546267.

Kampe, T.U., Johnson, B.R., Kuester, M., & Keller, M. (2010). NEON: The first continental-scale ecological observatory with airborne remote sensing of vegetation canopy biochemistry and structure. *Journal of Applied Remote Sensing*, *4*, 043510. http://dx.doi.org/10.1117/1.3361375.

Kergoat, L., Lafont, S., Arneth, A., Le Dantec, V., & Saugier, B. (2008). Nitrogen controls plant canopy light-use efficiency in temperate and boreal ecosystems. *Journal of Geophysical Research*, *113*, G04017. http://dx.doi.org/10.1029/2007JG000676.

King, D.A. (1997). The functional significance of leaf angle in *Eucalyptus*. *Australian Journal of Botany*, *45*, 619–639. http://dx.doi.org/10.1071/BT96063.

Kokaly, R.F., & Clark, R.N. (1999). Spectroscopic determination of leaf biochemistry using band-depth analysis of absorption features and stepwise multiple linear regression. *Remote Sensing of Environment*, *67*, 267–287. http://dx.doi.org/10.1016/S0034-4257(98)00084-4.

Kokaly, R.F., Asner, G.P., Ollinger, S.V., Martin, M.E., & Wessman, C.A. (2009). Characterizing canopy biochemistry from imaging spectroscopy and its application to ecosystem studies. *Remote Sensing of Environment*, *113*, S78–S91. http://dx.doi.org/10.1016/j.rse.2008.10.018.

Kruse, J.K., Christians, N.E., & Chaplin, M.H. (2006). Remote sensing of nitrogen stress in creeping bentgrass. *Agronomy Journal*, *98*, 1640–1645. http://dx.doi.org/10.2134/agronj2006.0022.

Litton, C.M., Raich, J.W., & Ryan, M.G. (2007). Carbon allocation in forest ecosystems. *Global Change Biology*, *13*, 2089–2109. http://dx.doi.org/10.1111/j.1365-2486.2007.01420.x.

Longstreth, D.J., Bolaños, J.A., & Goddard, R.H. (1985). Photosynthetic rate and mesophyll surface area in expanding leaves of *Alternanthera philoxeroides* grown at two light levels. *American Journal of Botany*, *72*, 14–19 (http://www.jstor.org/stable/2443564).

Martin, M.E., & Aber, J.D. (1997). High spectral resolution remote sensing of forest canopy lignin, nitrogen, and ecosystem processes. *Ecological Applications*, *7*, 431–443. http://dx.doi.org/10.1890/1051-0761(1997)007[0431:HSRRSO]2.0.CO;2.

Martin, M.E., Plourde, L.C., Ollinger, S.V., Smith, M. -L., & McNeil, B.E. (2008). A generalizable method for remote sensing of canopy nitrogen across a wide range of forest ecosystems. *Remote Sensing of Environment*, *112*, 3511–3519. http://dx.doi.org/10.1016/j.rse.2008.04.008.

Mattson, W.J. (1980). Herbivory in relation to plant nitrogen-content. *Annual Review of Ecology and Systematics*, *11*, 119–161. http://dx.doi.org/10.1146/annurev.es.11.110180.001003.

McNeil, B.E., Read, J.M., Sullivan, T.J., McDonnell, T.C., Fernandez, I.J., & Driscoll, C.T. (2008). The spatial pattern of nitrogen cycling in the Adirondack Park, New York. *Ecological Applications*, *18*, 438–452. http://dx.doi.org/10.1890/07-0276.1.

Merilä, P., & Derome, J. (2008). Relationships between needle nutrient composition in Scots pine and Norway spruce stands and the respective concentrations in organic layer and in percolation water. *Boreal Environment Research*, *13*(Suppl. B), 35–47.

Molotch, N.P., & Bales, R.C. (2006). Comparison of ground-based and airborne snow surface albedo parameterizations in an alpine watershed: Impact on snowpack mass balance. *Water Resources Research*, *42*, W05410. http://dx.doi.org/10.1029/2005WR004522.

Mouroulis, P., & McKerns, M.M. (2000). Pushbroom imaging spectrometer with high spectroscopic data fidelity: Experimental demonstration. *Optical Engineering*, *39*(3), 808–816. http://dx.doi.org/10.1117/1.602431.

Nigon, T.J., Rosen, C.J., Mulla, D.J., Cohen, Y., Alchanatis, V., & Rud, R. (2012). Hyperspectral imagery for the detection of nitrogen stress in potato for in-season management. *Proceedings of the 11th international conference on precision agriculture, [CD-ROM], Indianapolis, USA* (15 pp. https://www.ispag.org/abstract_papers/papers/abstract_1200.pdf).

Niinemets, Ü., Cescatti, A., Lukjanova, A., Tobias, M., & Truus, L. (2002). Modification of light-acclimation of *Pinus sylvestris* shoot architecture by site fertility. *Agricultural and Forest Meteorology*, *111*, 121–140.

Oak Ridge National Laboratory Distributed Active Archive Center (ORNL DAAC) (2011e). MODIS subsetted land products, Collection 5. Available on-line http://daac.ornl.gov/MODIS/modis.html from ORNL DAAC, Oak Ridge, Tennessee, U.S.A. Accessed September 12, 2011

Ollinger, S.V. (2011). Sources of variability in canopy reflectance and the convergent properties of plants. *New Phytologist*, *189*, 375–394. http://dx.doi.org/10.1111/j.1469-8137.2010.03536.x.

Ollinger, S.V., & Smith, M. -L. (2005). Net primary production and canopy nitrogen in a temperate forest landscape: An analysis using imaging spectroscopy, modeling and field data. *Ecosystems*, *8*, 760–778. http://dx.doi.org/10.1007/s10021-005-0079-5.

Ollinger, S.V., Richardson, A.D., Martin, M.E., Hollinger, D.Y., Frolking, S.E., Reich, P.B., ... Schmid, H.P. (2008). Canopy nitrogen, carbon assimilation, and albedo in temperate and boreal forests: Functional relations and potential climate feedbacks. *Proceedings of the National Academy of Sciences of the USA*, *105*, 19336–19341. http://dx.doi.org/10.1073/pnas.0810021105.

Ollinger, S.V., Smith, M.L., Martin, M.E., Hallett, R.A., Goodale, C.L., & Aber, J.D. (2002). Regional variation in foliar chemistry and soil nitrogen status among forests of diverse history and composition. *Ecology*, *83*, 339–355. http://dx.doi.org/10.2307/2680018.

Pacumbaba, R.O., & Beyl, C.A. (2011). Changes in hyperspectral reflectance signatures of lettuce leaves in response to macronutrient deficiencies. *Advances in Space Research*, *48*, 32–42. http://dx.doi.org/10.1016/j.asr.2011.02.020.

Parton, W., Silver, W.L., Burke, I.C., Grassens, L., Harmon, M.E., Currie, W.S., ... Fasth, B. (2007). Global scale similarities in nitrogen release patterns during long term decomposition. *Science*, *315*, 361–364. http://dx.doi.org/10.1126/science.1134853.

Peddle, D.R., Johnson, R.L., Cihlar, J., & Latifovic, R. (2004). Large area forest classification and biophysical parameter estimations using the 5-Scale canopy reflectance model in Multiple-Forward-Mode. *Remote Sensing of Environment*, *8*, 252–263. http://dx.doi.org/10.1016/j.rse.2002.08.001.

Peeters, P.J. (2002). Correlations between leaf constituent levels and the densities of herbivorous insect guilds in an Australian forest. *Austral Ecology*, *27*, 658–671. http://dx.doi.org/10.1046/j.1442-9993.2002.01227.x.

Platt, R.V., & Goetz, A.F.H. (2004). Comparison of AVIRIS and Landsat for land use classification at the urban fringe. *Photogrammetric Engineering & Remote Sensing*, *70*(7), 813–819. http://dx.doi.org/10.14358/PERS.70.7.813.

Plourde, L.C., Ollinger, S.V., Smith, M. -L., & Martin, M.E. (2007). Estimating species abundance in a northern temperate forest using spectral mixture analysis. *Photogrammatric Engineering & Remote Sensing*, *73*, 829–840. http://dx.doi.org/10.14358/PERS.73.7.829.

Pontius, J., Hallett, R., & Martin, M. (2005). Using AVIRIS to assess hemlock abundance and early decline in the Catskills, New York. *Remote Sensing of Environment*, *97*, 163–173. http://dx.doi.org/10.1016/j.rse.2005.04.011.

Posada, J.M., Lechowicz, M.J., & Kitajima, K. (2009). Optimal photosynthetic use of light by tropical tree crowns achieved by adjustment of individual leaf angles and nitrogen content. *Annals of Botany*, *103*, 795–805. http://dx.doi.org/10.1093/aob/mcn265.

Pringle, M.J., Schmidt, M., & Muir, J.S. (2009). Geostatistical interpolation of SLC-off Landsat ETM plus images. *ISPRS Journal of Photogrammetry and Remote Sensing*, *64*, 654–664. http://dx.doi.org/10.1016/j.isprsjprs.2009.06.001.

Pu, R. (2009). Broadleaf species recognition with *in situ* hyperspectral data. *International Journal of Remote Sensing*, *30*, 2759–2779. http://dx.doi.org/10.1080/01431160802555820.

Rautiainen, M., Mõttus, M., Stenberg, P., & Ervasti, S. (2008). Crown envelope shape measurements and models. *Silva Fennica*, *42*, 19–33. http://dx.doi.org/10.14214/sf.261.

Reich, P.B., Ellsworth, D.S., Walters, M.B., Vose, J.M., Gresham, C., Volin, J.C., & Bowman, W.D. (1999). Generality of leaf trait relationships: A test across six biomes. *Ecology*, *806*, 1955–1966. http://dx.doi.org/10.1890/0012-9658(1999)080[1955:GOLTRA]2.0.CO;2.

Reich, P.B., Kloeppel, B.D., Ellsworth, D.S., & Walters, M.B. (1995). Different photosynthesis–nitrogen relations in deciduous hardwood and evergreen coniferous tree species. *Oecologia*, *104*, 24–30. http://dx.doi.org/10.1007/BF00365558.

Roberts, D.A., Ustin, S.L., Ogunjemiyo, S., Greenberg, J., Dobrowski, S.Z., Chen, J., & Hinckley, T.M. (2004). Spectral and structural measures of northwest forest vegetation at leaf to landscape scales. *Ecosystems*, *7*, 545–562. http://dx.doi.org/10.1007/s10021-004-0144-5.

Roy, D.P., Wulder, M.A., Loveland, T.R., Woodcock, C.E., Allen, R.G., Anderson, M.C., ... Zhu, Z. (2014). Landsat-8: Science and product vision for terrestrial global change research. *Remote Sensing of Environment*, *145*, 154–172. http://dx.doi.org/10.1016/j.rse.2014.02.001.

Schaaf, C.B., Gao, F., Strahler, A.H., Lucht, W., Li, X., Tsang, T., ... Roy, D. (2002). First operational BRDF, albedo nadir reflectance products from MODIS. *Remote Sensing of Environment*, *83*, 135–148. http://dx.doi.org/10.1016/S0034-4257(02)00091-3.

Serrano, L., Filella, I., & Peñuelas, J. (2000). Remote sensing of biomass and yield of winter wheat under different nitrogen supplies. *Crop Science*, *40*, 723–731. http://dx.doi.org/10.2135/cropsci2000.403723x.

Slaton, M.R., Hunt, E.R., Jr., & Smith, W.K. (2001). Estimating near-infrared leaf reflectance from leaf structural characteristics. *American Journal of Botany*, *88*(2), 278–284. http://dx.doi.org/10.2307/2657019.

Smith, M. -L., & Martin, M.E. (2001). A plot-based method for rapid estimation of forest canopy chemistry. *Canadian Journal of Forest Research*, *31*, 549–555. http://dx.doi.org/10.1139/cjfr-31-3-549.

Smith, M. -L., Martin, M.E., Plourde, L., & Ollinger, S.V. (2003). Analysis of hyperspectral data for estimation of temperate forest canopy nitrogen concentration: Comparison between an airborne (AVIRIS) and a spaceborne (Hyperion) sensor. *IEEE Transactions on Geoscience and Remote Sensing*, *41*, 1332–1337. http://dx.doi.org/10.1109/TGRS.2003.813128.

Smith, M. -L., Ollinger, S.V., Martin, M.E., Aber, J.D., Hallett, R.A., & Goodale, C.L. (2002). Direct estimation of aboveground forest productivity through hyperspectral remote sensing of canopy nitrogen. *Ecological Applications*, *12*, 1286–1302. http://dx.doi.org/10.2307/3099972.

Suárez, L., Zarco-Tejada, P.J., Supulcre-Cantó, G., Pérez-Priego, O., Miller, J.R., Jiménez-Muñoz, J.C., & Sobrino, J. (2008). Assessing canopy PRI for water stress detection with diurnal airborne imagery. *Remote Sensing of Environment*, *112*, 560–575. http://dx.doi.org/10.1016/j.rse.2007.05.009.

Townsend, P., Foster, J.R., Chastain, R.A., Jr., & Currie, W.S. (2003). Application of imaging spectroscopy to mapping canopy nitrogen in the forests of the central Appalachian Mountains using Hyperion and AVIRIS. *IEEE Transactions on Geoscience and Remote Sensing*, *41*, 1347–1354. http://dx.doi.org/10.1109/TGRS.2003.813205.

Underwood, E.C., Mulitsch, M.J., Greenberg, J.A., Whiting, M.L., Ustin, S.L., & Kefauver, S.C. (2006). Mapping invasive aquatic vegetation in the Sacramento–San Joaquin Delta using hyperspectral imagery. *Environmental Monitoring and Assessment*, *121*, 47–64. http://dx.doi.org/10.1007/s10661-005-9106-4.

Valiente-Banuet, A., Verdú, M., Valladares, F., & García-Fayos, P. (2010). Functional and evolutionary correlations of steep leaf angles in the mexical shrubland. *Oecologia*, *163*, 25–33. http://dx.doi.org/10.1007/s00442-009-1520-9.

Vitousek, P.M., & Howarth, R.W. (1991). Nitrogen limitation on land and in the sea: How can it occur? *Biogeochemistry*, *13*, 87–115 (Stable URL: http://www.jstor.org/stable/1468901).

Wang, J., Xu, R., & Yang, S. (2009). Estimation of plant water content by spectral absorption features centered at 1,450 nm and 1,940 nm regions. *Environmental Monitoring and Assessment*, 157–459. http://dx.doi.org/10.1007/s10661-008-0548-3 (-469).

Wessman, C.A., Aber, J.D., Peterson, D.L., & Melillo, J.M. (1988). Remote sensing of canopy chemistry and nitrogen cycling in temperate forest ecosystems. *Nature*, *335*, 154–156. http://dx.doi.org/10.1038/335154a0.

Wright, I.J., Reich, P.B., Westoby, M., Ackerly, D.D., Baruch, Z., Bongers, F., ... Villar, R. (2004). The worldwide leaf economics spectrum. *Nature*, *428*, 821–827. http://dx.doi.org/10.1038/nature02403.

Wythers, K.R., Reich, P.B., Tjoelker, M.G., & Bolstad, P.B. (2005). Foliar respiration acclimation to temperature and temperature variable Q_{10} alter ecosystem carbon balance. *Global Change Biology*, *11*, 435–449. http://dx.doi.org/10.1111/j.1365-2486.2005.00922.x.

Xiong, X., Angal, A., & Xie, X. (2008). On-orbit noise characterization for MODIS reflective solar bands. *IEEE IGARSS*, *4*, 1336–1339.

Zhang, Q., Xiao, X., Braswell, B., Linder, E., Ollinger, S., Smith, M. -L., ... Minocha, R. (2006). Characterization of seasonal variation in forest canopy in a temperate deciduous broadleaf forest, using daily MODIS data. *Remote Sensing of Environment*, *105*, 189–203. http://dx.doi.org/10.1016/j.rse.2006.06.013.

Zhao, C.J., Liu, L.Y., Wang, J.H., Huangm, W.J., Song, X.Y., & Li, C.J. (2005). Predicting grain protein content of winter wheat using remote sensing data based on nitrogen status and water stress. *International Journal of Applied Earth Observation and Geoinformation*, *7*, 1–9. http://dx.doi.org/10.1016/j.jag.2004.10.002.

Zygielbaum, A.I., Gitelson, A.A., Arkebauer, T.J., & Rundquist, D.C. (2009). Nondestructive detection of water stress and estimation of relative water content in maize. *Geophysical Research Letters*, *36*, L124. http://dx.doi.org/10.1029/2009GL038906.